

Spinning Spacecraft Attitude Estimation Using Markley Variables: Filter Implementation And Results^{*}

Joseph E. Sedlak

a.i. solutions, Inc., 10001 Dereewood Lane, Suite 215, Lanham, MD 20706 USA

E-mail: sedlak@ai-solutions.com

Abstract

Attitude estimation is often more difficult for spinning spacecraft than for three-axis stabilized platforms due to the need to follow rapidly-varying state vector elements and the lack of three-axis rate measurements from gyros. The estimation problem simplifies when torques are negligible and nutation has damped out, but the general case requires a sequential filter with dynamics propagation. This paper describes the implementation and test results for an extended Kalman filter for spinning spacecraft attitude and rate estimation based on a novel set of variables suggested in a paper by Markley [AAS 93-330] (referred to hereafter as Markley variables).

Markley has demonstrated that the new set of variables provides a superior parameterization for numerical integration of the attitude dynamics for spinning or momentum-biased spacecraft. The advantage is that the Markley variables have fewer rapidly-varying elements than other representations such as the attitude quaternion and rate vector. A filter based on these variables was expected to show improved performance due to the more accurate numerical state propagation. However, for a variety of test cases, it has been found that the new filter, as currently implemented, does not perform significantly better than a quaternion-based filter that was developed and tested in parallel.

This paper reviews the mathematical background for a filter based on Markley variables. It also describes some features of the implementation and presents test results. The test cases are based on a mission using magnetometer and Sun sensor data and gyro measurements on two axes normal to the spin axis. The orbit and attitude scenarios and spacecraft parameters are modeled after one of the THEMIS (Time History of Events and Macroscale Interactions during Substorms) probes.

Several tests are presented that demonstrate the filter accuracy and convergence properties. The tests include torque-free motion with various nutation angles, large constant-torque attitude slews, sensor misalignments, large initial attitude and rate errors, and cases with low data frequency. It is found that the convergence is rapid, the radius of convergence is large, and the results are reasonably accurate even in the presence of unmodeled perturbations.

INTRODUCTION

There are many ways to represent spacecraft attitude and its time rate of change. One representation has been put forward as superior in some respects for spinning or momentum-biased spacecraft. Markley (Ref. 1) has presented a new set of variables that have fewer rapidly varying elements for spinning spacecraft than other commonly used representations. For this reason they provide numerical advantages when integrating the equations of motion. An earlier paper (Ref. 2) presented the mathematical background for an extended Kalman filter (EKF) designed to estimate spacecraft attitude using these new variables. The current paper draws heavily from Ref. 2 for a review of that background, with corrections, and then describes new work on the filter implementation and test results.

Attitude estimation methods for non-spinning, three-axis stabilized spacecraft often make use of the Euler symmetric parameters (commonly called the quaternion) to represent the attitude (Ref. 3) with respect to an inertial reference frame. The quaternion is a four-component, globally nonsingular attitude representation. The state vector typically has seven components consisting of the quaternion plus three elements that provide bias corrections to the measured rates. Spinning spacecraft usually do not carry three-axis rate-sensing gyros, so the rotation rate vector

*

This work was supported by the National Aeronautics and Space Administration (NASA) / Goddard Space Flight Center (GSFC), Greenbelt, MD, USA, Contract NNG04DA01C.

NASA/GSFC, Mission Engineering and Systems Analysis Division, *Flight Mechanics Symposium*, Greenbelt, MD, Oct. 2005.

itself must be estimated rather than just the biases. Rates are needed for numerical time-propagation since the differential equation describing the attitude dynamics is 2nd-order in time. A disadvantage of this state representation is that all four quaternion components and two of the body frame rate components are varying even for the simple case of torque-free nutating motion. As shown in Ref. 1, alternative descriptions can be devised that have as few as three varying elements for this case, and thus, are easier to integrate numerically. These alternative representations will be referred to here as Markley variables.

The goal of the current work is to design and build a Kalman filter for attitude estimation using the Markley variables. This new filter has been fully developed and incorporated into the attitude ground support system used for spinning spacecraft at the NASA Goddard Space Flight Center. In addition, a second new filter has been developed for comparison. This second filter is a more conventional EKF based on the quaternion and body rotation rate rather than Markley variables. It is found that the two filters have very similar performance; the Markley variable filter, as currently implemented, is not significantly more accurate than the quaternion and rate filter.

The Markley variables are defined in Section 2. Section 3 reviews the partial derivatives required for a Kalman filter based on these variables. In particular, the observation partials are needed for the sensitivity matrix, and the linearized dynamics matrix is needed for time-propagation of the covariance matrix. Section 4 describes how the constraint condition can be explicitly incorporated in the filter equations, yielding a reduction of the filter update and the covariance matrix from 7 to 6 dimensions. Section 5 presents several numerical tests using simulated data patterned after the THEMIS spacecraft. Comparisons are made with a more typical EKF based on the quaternion and body rotation rate. Section 6 gives some conclusions.

MARKLEY VARIABLES

The seven variables of the attitude dynamics representation described in Ref. 1 are:

- the angular momentum, \mathbf{L}_I , in an inertial reference frame (typically, the geocentric inertial (GCI) frame),
- the angular momentum, \mathbf{L}_B , in the body frame,
- and a rotation angle, ζ , defined below.

(Bold characters will be used throughout to denote 3-vectors.) A constraint condition holds for these variables: the magnitude of the angular momentum vector must be the same in the inertial and instantaneous body frames.

The angle ζ can be defined in a number of different ways. In this work, Markley's second representation is used, as follows. An intermediate frame is defined by rotating the inertial frame angular momentum into the body frame angular momentum, treating these as distinct vectors rather than as two representations of the same abstract vector. (Or, saying this more carefully, one transforms \mathbf{L}_I into a frame where its components happen to be the same as those of \mathbf{L}_B .) The usual attitude matrix is only one of an infinite set of possible transformations that carry \mathbf{L}_I into \mathbf{L}_B . The intermediate frame here is defined as the one obtained by choosing the most direct path from \mathbf{L}_I to \mathbf{L}_B . For this purpose, the rotation vector is in the direction of the cross product $\mathbf{L}_I \times \mathbf{L}_B$. Call this transformation from the inertial frame to the intermediate frame A_{EI} . Then, it can be shown that the transformation from the intermediate frame to the body, A_{BE} , is simply a rotation about \mathbf{L}_B , as follows.

The attitude matrix, A_{BI} , is the transformation from the inertial to the body frame; thus,

$$A_{BI} \mathbf{L}_I = \mathbf{L}_B . \quad (1)$$

By construction of A_{EI} , it is also true that

$$A_{EI} \mathbf{L}_I = \mathbf{L}_B . \quad (2)$$

The transformation, A_{BE} , is defined such that $A_{BE} A_{EI} = A_{BI}$. Hence, one can write

$$A_{BE} A_{EI} \mathbf{L}_I = A_{BI} \mathbf{L}_I , \quad (3)$$

and this becomes

$$A_{BE} \mathbf{L}_B = \mathbf{L}_B . \quad (4)$$

Thus, \mathbf{L}_B is an eigenvector of the orthogonal matrix A_{BE} . Equivalently, \mathbf{L}_B is the Euler rotation axis for the transformation A_{BE} . The corresponding Euler rotation angle defines the 7th Markley variable, ζ . With this definition, A_{BE} can be written (Ref. 3)

$$A_{BE} = \cos \zeta I + \frac{1 - \cos \zeta}{L^2} \mathbf{L}_B \mathbf{L}_B^T - \frac{\sin \zeta}{L} [\mathbf{L}_B \times], \quad (5)$$

where I is the 3×3 identity matrix, and the cross-product matrix is defined for any vector \mathbf{v} to be

$$[\mathbf{v} \times] \equiv \begin{bmatrix} 0 & -v_z & v_y \\ v_z & 0 & -v_x \\ -v_y & v_x & 0 \end{bmatrix}. \quad (6)$$

(Properties of the cross-product matrix are extensively described in Ref. 3.) The angle ζ is the rotation about \mathbf{L}_B to get from the intermediate frame to the body frame, and thus, represents predominantly the spin phase.

Equations of Motion

The Kalman filter requires expressions for the time-dependence of the state vector. The equation of motion for the angular momentum in the inertial frame is

$$\frac{d\mathbf{L}_I}{dt} = \mathbf{N}_I, \quad (7)$$

where \mathbf{N}_I is the total external torque. This equation expressed in the body frame is

$$\frac{d\mathbf{L}_B}{dt} = \mathbf{N}_B - \boldsymbol{\omega}_{BI} \times \mathbf{L}_B, \quad (8)$$

where

$$\boldsymbol{\omega}_{BI} = J^{-1}(\mathbf{L}_B - \mathbf{h}_B) \quad (9)$$

is the body rotation rate vector, J is the spacecraft moment of inertia tensor, and \mathbf{h}_B is the angular momentum relative to the body frame of any internal moving components. The external torque expressed in the body frame is

$$\mathbf{N}_B = A_{BI} \mathbf{N}_I. \quad (10)$$

Reference 1 shows that the time-dependence of the phase angle, ζ , satisfies the equation

$$\frac{d\zeta}{dt} = \frac{L [(\mathbf{L}_B + \mathbf{L}_I) \cdot \boldsymbol{\omega}_{BI} + L^{-2} (\mathbf{L}_B \times \mathbf{L}_I) \cdot (\mathbf{N}_B + \mathbf{N}_I)]}{L^2 + \mathbf{L}_B \cdot \mathbf{L}_I}. \quad (11)$$

KALMAN FILTER

This section discusses the main parts of the Kalman filter. These are the propagation step and the update step for both the state vector and the state covariance matrix. Other details about Kalman filtering can be found, for example, in Ref. 4, with specific application to spacecraft attitude quaternion estimation in Ref. 5.

Time Propagation

The equations of motion can be integrated numerically to propagate the full 7-component state forward in time between sensor observations. As currently implemented, the integrator uses a 4th-order Runge-Kutta method, with

options to express the total torque as a sum of the command torques and environmental torques from gravity gradient and residual magnetization perturbations.

The state error covariance is defined as the expectation value of the outer product of the errors in the state, $P = E[(X - \bar{X})(X - \bar{X})^T]$, where \bar{X} is the expectation value of the state. The covariance P is a 7×7 matrix; however, since the norms of \mathbf{L}_B and \mathbf{L}_I are constrained to be equal, P is of rank 6 for an optimal estimator. Anticipating this problem and the resolution that will be given below, the full state vector now is defined to be

$$X \equiv \begin{bmatrix} \hat{\mathbf{L}}_I \\ \mathbf{L}_B \\ \zeta \end{bmatrix}, \quad (12)$$

where $\hat{\mathbf{L}}_I$ is the unit vector in the direction of the inertial frame angular momentum. This state still has seven components, but the constraint now is that the first three elements have unit norm.

The 7×7 error covariance satisfies the equation

$$\frac{dP}{dt} = FP + PF^T + Q(t), \quad (13)$$

where $Q(t)$ is the process noise (Ref. 4), and F is obtained from the state dynamics equation,

$$\frac{dX}{dt} = f(X, t), \quad (14)$$

with

$$F \equiv \frac{\partial f(X, t)}{\partial X} \quad (15)$$

evaluated at the current state estimate. The function $f(X, t)$ is given by Eqs. 7, 8, and 11, except Eq. 7 now becomes

$$\frac{d\hat{\mathbf{L}}_I}{dt} = (I - \hat{\mathbf{L}}_I \hat{\mathbf{L}}_I^T) \frac{\mathbf{N}_I}{L} \quad (16)$$

to account for the unitized inertial frame angular momentum in Eq. 12. With this change, the expression for F is

$$F = \begin{bmatrix} -(\hat{\mathbf{L}}_I \cdot \mathbf{N}_I I + \hat{\mathbf{L}}_I \mathbf{N}_I^T) / L & -(I - \hat{\mathbf{L}}_I \hat{\mathbf{L}}_I^T) \mathbf{N}_I \mathbf{L}_B^T / L^3 & \mathbf{0}_{3 \times 1} \\ \mathbf{0}_{3 \times 3} & [\mathbf{L}_B \times] J^{-1} - [J^{-1} \mathbf{L}_B \times] & \mathbf{0}_{3 \times 1} \\ d_I L / (L^2 + \mathbf{L}_I \cdot \mathbf{L}_B) & d_B L / (L^2 + \mathbf{L}_I \cdot \mathbf{L}_B) & \mathbf{0}_{1 \times 1} \end{bmatrix}, \quad (17)$$

with

$$d_I = -\mathbf{L}_B^T \frac{d\zeta}{dt} + L (J^{-1} \mathbf{L}_B)^T + (\mathbf{N}_B + \mathbf{N}_I)^T [\hat{\mathbf{L}}_B \times] \quad (18)$$

and

$$\begin{aligned} d_B = & -(\hat{\mathbf{L}}_B + \hat{\mathbf{L}}_I)^T \frac{d\zeta}{dt} + (J^{-1} \mathbf{L}_B)^T - (\mathbf{N}_B + \mathbf{N}_I)^T [\hat{\mathbf{L}}_I \times] / L \\ & + (\mathbf{L}_B + \mathbf{L}_I)^T J^{-1} + (\hat{\mathbf{L}}_I \cdot J^{-1} \hat{\mathbf{L}}_B) \mathbf{L}_B^T \\ & - (\hat{\mathbf{L}}_B \times \hat{\mathbf{L}}_I) \cdot (\mathbf{N}_B + \mathbf{N}_I) \hat{\mathbf{L}}_B^T / L. \end{aligned} \quad (19)$$

Sensitivity Matrix

The sensitivity, H , is defined as the matrix of partials of the sensor observation with respect to the state X . This matrix is constructed in this section by chaining together partial derivatives with respect to intermediate variables. The current filter implementation is designed to accept observations from vector sensors, quaternion sensors (such as autonomous star trackers), or rate measurements from 1-, 2-, or 3-axis gyros. This section discusses H for vector and rate measurements.

Vector observations, for example, may be obtained from a three-axis magnetometer or constructed from the output of an Earth sensor or a V-slit Sun or star sensor. It is assumed the vector observations have been transformed to the body frame where they are modeled as

$$\begin{aligned} \mathbf{v}_B^{obs} &= A_{BI} \mathbf{v}_I + \mathbf{n} \\ &= \exp([\boldsymbol{\alpha} \times]) A_{est} \mathbf{v}_I + \mathbf{n} \\ &\approx (I + [\boldsymbol{\alpha} \times]) \mathbf{v}_B \\ &= \mathbf{v}_B - [\mathbf{v}_B \times] \boldsymbol{\alpha} \quad , \end{aligned} \tag{20}$$

where \mathbf{v}_I and \mathbf{v}_B are the reference vector expressed in the inertial frame and body frame, respectively, A_{est} is the current estimate of the attitude matrix, $\boldsymbol{\alpha}$ is the negative of the unknown attitude error vector, and \mathbf{n} represents random noise with covariance R . Thus, the partial of \mathbf{v}_B^{obs} with respect to $\boldsymbol{\alpha}$ is $-[\mathbf{v}_B \times]$. Using $\boldsymbol{\alpha}$ in the error state rather than $-\boldsymbol{\alpha}$ simplifies signs elsewhere when constructing a quaternion-based filter.

The partial of $\boldsymbol{\alpha}$ with respect to the quaternion is related to the Ξ matrix in Ref. 5 and can be shown to be

$$\frac{\partial \boldsymbol{\alpha}}{\partial \mathbf{q}} = -\frac{1}{2} \begin{bmatrix} q_4 & q_3 & -q_2 & -q_1 \\ -q_3 & q_4 & q_1 & -q_2 \\ q_2 & -q_1 & q_4 & -q_3 \end{bmatrix} . \tag{21}$$

Next, the attitude quaternion can be expressed as a function of the Markley variables, X , and the partials of the vector part of the quaternion, \mathbf{q} , with respect to X can be determined. This yields

$$\frac{\partial \mathbf{q}}{\partial \hat{\mathbf{L}}_I} = \frac{C_1 \cos(\zeta/2)}{L \sqrt{2(L^2 + \mathbf{L}_I \cdot \mathbf{L}_B)}} + \frac{C_2 \sin(\zeta/2)}{\sqrt{2(L^2 + \mathbf{L}_I \cdot \mathbf{L}_B)}} , \tag{22}$$

$$\frac{\partial \mathbf{q}}{\partial \mathbf{L}_B} = \frac{C_3 \cos(\zeta/2)}{L \sqrt{2(L^2 + \mathbf{L}_I \cdot \mathbf{L}_B)}} + \frac{C_4 \sin(\zeta/2)}{\sqrt{2(L^2 + \mathbf{L}_I \cdot \mathbf{L}_B)}} , \tag{23}$$

and

$$\frac{\partial \mathbf{q}}{\partial \zeta} = -\frac{(\mathbf{L}_B \times \mathbf{L}_I) \sin(\zeta/2)}{2L \sqrt{2(L^2 + \mathbf{L}_I \cdot \mathbf{L}_B)}} + \frac{(\mathbf{L}_B + \mathbf{L}_I) \cos(\zeta/2)}{2 \sqrt{2(L^2 + \mathbf{L}_I \cdot \mathbf{L}_B)}} , \tag{24}$$

where

$$C_1 = -\frac{(\mathbf{L}_B \times \mathbf{L}_I) L \mathbf{L}_B^T / 2}{L^2 + \mathbf{L}_I \cdot \mathbf{L}_B} + L [\mathbf{L}_B \times] , \tag{25}$$

$$C_2 = -\frac{(\mathbf{L}_B + \mathbf{L}_I) L \mathbf{L}_B^T / 2}{L^2 + \mathbf{L}_I \cdot \mathbf{L}_B} + L I , \tag{26}$$

$$C_3 = -\frac{(\mathbf{L}_B \times \mathbf{L}_I) \left(\mathbf{L}_B + \frac{\mathbf{L}_I}{2} + \frac{\mathbf{L}_B \cdot \mathbf{L}_I}{2L^2} \mathbf{L}_B \right)^T}{L^2 + \mathbf{L}_I \cdot \mathbf{L}_B} - [\mathbf{L}_I \times] , \tag{27}$$

and

$$C_4 = I + \frac{\mathbf{L}_I \mathbf{L}_B^T}{L^2} - \frac{(\mathbf{L}_B + \mathbf{L}_I) \left(\mathbf{L}_B + \frac{\mathbf{L}_I}{2} + \frac{\mathbf{L}_B \cdot \mathbf{L}_I}{2L^2} \mathbf{L}_B \right)^T}{L^2 + \mathbf{L}_I \cdot \mathbf{L}_B}. \quad (28)$$

The partial of the 4th-component of q is

$$\frac{\partial q_4}{\partial X} = \frac{1}{2^{3/2} (L^2 + \mathbf{L}_I \cdot \mathbf{L}_B)^{1/2}} \left[\cos(\zeta/2) \mathbf{L}_B^T, \cos(\zeta/2) \hat{\mathbf{L}}_I^T (\mathbf{I} - \hat{\mathbf{L}}_B \hat{\mathbf{L}}_B^T), -\sin(\zeta/2) \frac{L^2 + \mathbf{L}_I \cdot \mathbf{L}_B}{L} \right]. \quad (29)$$

The 3×7 sensitivity matrix for vector observations is obtained by combining these pieces using the chain rule,

$$H = \frac{\partial \mathbf{v}_B^{obs}}{\partial X} = -[\mathbf{v}_B \times] \left(\frac{\partial \boldsymbol{\alpha}}{\partial q} \right) \left[\frac{\partial q}{\partial \hat{\mathbf{L}}_I}, \frac{\partial q}{\partial \mathbf{L}_B}, \frac{\partial q}{\partial \zeta} \right]. \quad (30)$$

This expression is evaluated approximately using the current state estimate on the right-hand side.

Note that Eqs. 19 through 30 have been corrected and differ slightly from Ref. 2. All the partial derivatives have now been validated by extensive numerical tests.

For rate observations, the actual measurements are the projections of the true spacecraft rotation rate along the sensitive axis of each gyro unit. (It is assumed that any bias, scale factor, or misalignment corrections have already been applied. Calibration methods are a topic of ongoing work.) If there are three sensitive axes, aligned with the unit vectors \mathbf{U}_1 , \mathbf{U}_2 , and \mathbf{U}_3 , then the sensor frame rate observations are simply $\mathbf{U}_i \cdot \boldsymbol{\omega}_{BI}$ plus noise, for $i=1$ to 3. As indicated by Eq. 9, the partial derivative with respect to the Markley variables is nonzero only for \mathbf{L}_B , thus

$$H = \frac{\partial}{\partial X} \begin{bmatrix} \mathbf{U}_1 \cdot \boldsymbol{\omega}_{BI} \\ \mathbf{U}_2 \cdot \boldsymbol{\omega}_{BI} \\ \mathbf{U}_3 \cdot \boldsymbol{\omega}_{BI} \end{bmatrix} = [0_{3 \times 3} \quad U_J \quad 0_{3 \times 1}], \quad (31)$$

where

$$U_J \equiv \begin{bmatrix} \mathbf{U}_1^T \\ \mathbf{U}_2^T \\ \mathbf{U}_3^T \end{bmatrix} J^{-1}. \quad (32)$$

If there are fewer than three gyro axes, H is obtained by deleting the appropriate rows from Eq. 31.

REDUCED REPRESENTATION

Knowledge of the 7×7 state error covariance derives from an a priori estimate plus updates based on sensor observations. This information should account for the constraint condition at each step. If this is the case, the covariance matrix will have rank 6. Any treatment where the covariance has rank 7 must be using the initialization or update information sub-optimally.

It can be difficult numerically to maintain the covariance P as a rank 6 matrix during the filter propagation and update steps. To avoid this problem entirely, it is preferable to recast the filter in terms of a 6-component error state, reducing the dimensionality of the covariance matrix and the filter update.

The state reduction depends on two facts. First, as given in Eq. 12, the first three components of the state are taken to be the *unit vector* in the direction of \mathbf{L}_I rather than \mathbf{L}_I itself. Second, the filter update step will affect only the components perpendicular to the a priori angular momentum; the parallel component is affected only in 2nd-order because it is a unit vector. Thus, any reference to the component parallel to \mathbf{L}_I can be discarded, reducing the dimensionality of the state by one.

The rest of this section gives the details needed to define the reduced state and to use it to create a reduced representation of the filter.

Unit Vector Covariance

The 3×3 submatrix of P corresponding to the uncertainty in the unit vector angular momentum can be related to the covariance corresponding to the 3-vector L_I as follows. Let the angular momentum and its error be written

$$\mathbf{L}' = \mathbf{L} + \delta\mathbf{L} , \quad (33)$$

where $\delta\mathbf{L}$ has zero mean. Then, the corresponding unit vector and its error are

$$\begin{aligned} \hat{\mathbf{L}}' &= (\mathbf{L} + \delta\mathbf{L}) \left(L^2 + 2\delta\mathbf{L} \cdot \mathbf{L} + \delta L^2 \right)^{-1/2} \\ &\approx \hat{\mathbf{L}} + \left(I - \hat{\mathbf{L}}\hat{\mathbf{L}}^T \right) \frac{\delta\mathbf{L}}{L} , \end{aligned} \quad (34)$$

where the subscript I has been dropped here for simplicity. The angular momentum covariance is

$$P_L = E[\delta\mathbf{L}\delta\mathbf{L}^T] , \quad (35)$$

and, from Eq. 34, the covariance of the unitized angular momentum vector is

$$P_{\hat{\mathbf{L}}} \approx L^{-2} \left(I - \hat{\mathbf{L}}\hat{\mathbf{L}}^T \right) P_L \left(I - \hat{\mathbf{L}}\hat{\mathbf{L}}^T \right) . \quad (36)$$

This property will be used below.

Reduction to 6-Component State

Next, construct the matrix M^T that rotates L_I to be parallel to the Z -axis of the inertial frame. With this transformation, it is possible to reduce the dimensionality of the state simply by discarding the third component of $M^T \hat{\mathbf{L}}_I$, which is manifestly equal to unity. Only the X - and Y - components are kept since they can deviate from zero in the 1st order at the update step of the filter.

To this end, define

$$M \equiv I \cos \vartheta + (1 - \cos \vartheta) \hat{\mathbf{n}}\hat{\mathbf{n}}^T + \sin \vartheta [\hat{\mathbf{n}} \times] , \quad (37)$$

where ϑ is the angle between the Z -axis and L_I , and

$$\hat{\mathbf{n}} = \frac{\hat{\mathbf{Z}} \times \hat{\mathbf{L}}_I}{|\hat{\mathbf{Z}} \times \hat{\mathbf{L}}_I|} . \quad (38)$$

With this definition, one has

$$M \hat{\mathbf{Z}} = \hat{\mathbf{L}}_I , \quad (39)$$

by construction. Also, define the matrices

$$m_{23} \equiv \begin{bmatrix} 1 & 0 & 0 \\ 0 & 1 & 0 \end{bmatrix} , \quad m_{32} \equiv \begin{bmatrix} 1 & 0 \\ 0 & 1 \\ 0 & 0 \end{bmatrix} \quad (40)$$

that actually perform the change of dimensionality. One can show that

$$M m_{32} m_{23} M^T = I - \hat{\mathbf{L}}_I \hat{\mathbf{L}}_I^T . \quad (41)$$

Now, define the 6-component state to be

$$x \equiv \begin{bmatrix} m_{23} M^T \hat{\mathbf{L}}_l \\ \mathbf{L}_B \\ \zeta \end{bmatrix} = S^T X , \quad (42)$$

where S^T is the 6×7 matrix

$$S^T \equiv \begin{bmatrix} m_{23} M^T & 0_{2 \times 3} & 0_{2 \times 1} \\ 0_{3 \times 3} & I & 0_{3 \times 1} \\ 0_{1 \times 3} & 0_{1 \times 3} & 1 \end{bmatrix} . \quad (43)$$

The m_{23} matrix in Eq. 42 explicitly removes the Z-component of the rotated unit angular momentum vector. Equation 42 also shows that

$$\frac{\partial x}{\partial X} = S^T . \quad (44)$$

Two important properties of the S matrix are that $S^T S = I_{6 \times 6}$, and, using Eq. 41,

$$I_{7 \times 7} = S S^T + Z_L . \quad (45)$$

In these expressions, $I_{6 \times 6}$ and $I_{7 \times 7}$ are the 6×6 and 7×7 identity matrices, and the 7×7 matrix Z_L is defined as

$$Z_L \equiv \begin{bmatrix} \hat{\mathbf{L}}_l \hat{\mathbf{L}}_l^T & 0_{3 \times 3} & 0_{3 \times 1} \\ 0_{3 \times 3} & 0_{3 \times 3} & 0_{3 \times 1} \\ 0_{1 \times 3} & 0_{1 \times 3} & 0_{1 \times 1} \end{bmatrix} . \quad (46)$$

Reduced Form for the Filter

The 6×6 covariance matrix for the reduced state now can be defined as

$$\bar{P} \equiv S^T P S \quad (47)$$

(overbar indicates 6-component reduced form). From Eq. 13, the time derivative is

$$\begin{aligned} \frac{d\bar{P}}{dt} &\approx S^T \frac{dP}{dt} S \\ &= S^T F (S S^T + Z_L) P S \\ &\quad + S^T P (S S^T + Z_L) F^T S + S^T Q(t) S , \end{aligned} \quad (48)$$

where the identity $I_{7 \times 7}$ has been introduced in the form given in Eq. 45. The time-dependence of S has been neglected. In the absence of external torques, S is exactly constant, and in practice, the variation is small over each short numerical integration interval. Recomputing S once for each time step should be sufficiently accurate for propagation of the covariance.

Note that

$$P Z_L = Z_L P = 0 \quad (49)$$

since L_I in Z_L is annihilated by the unit vector covariance, as given by Eq. 36. Thus, if one defines

$$\bar{F} \equiv S^T F S \quad (50)$$

and

$$\bar{Q} \equiv S^T Q S , \quad (51)$$

then Eq. 48 reduces to

$$\frac{d\bar{P}}{dt} = \bar{F}\bar{P} + \bar{P}\bar{F}^T + \bar{Q}(t) . \quad (52)$$

This is of the same standard form as Eq. 13 and carries the same information content but is not subject to any constraint condition.

Similarly, the 7×3 Kalman gain

$$K = PH^T (HPH^T + R)^{-1} \quad (53)$$

can be written in a reduced 6×3 form by introducing $I_{7 \times 7}$ expressed as in Eq. 45. Thus,

$$\begin{aligned} S^T K &= S^T P (SS^T + Z_L) H^T [H(SS^T + Z_L)P(SS^T + Z_L)H^T + R]^{-1} \\ &= \bar{P}\bar{H}^T [\bar{H}\bar{P}\bar{H}^T + R]^{-1} \\ &\equiv \bar{K} , \end{aligned} \quad (54)$$

where R is the covariance of the sensor noise, \mathbf{n} , in Eq. 20, and where the reduced 3×6 sensitivity matrix is

$$\bar{H} \equiv H S . \quad (55)$$

Finally, the state update is

$$\delta x = \bar{K} (\mathbf{v}_B^{obs} - \mathbf{v}_B^{ref}) . \quad (56)$$

The 3rd, 4th, and 5th elements of the update vector δx are added to the a priori estimate of L_B . The 6th element of δx is added to the a priori estimate of ζ . The 1st and 2nd elements of δx are corrections to the unitized angular momentum vector in the rotated frame; the corresponding a priori elements of x are zero by construction. Thus, the updated inertial frame angular momentum unit vector is

$$\hat{L}_I = M \begin{bmatrix} \delta x_1 \\ \delta x_2 \\ 1 \end{bmatrix} (1 + \delta x_1^2 + \delta x_2^2)^{-1/2} , \quad (57)$$

where M is given by Eq. 37. The full vector L_I can be recovered at any time from \hat{L}_I and the norm of L_B .

In summary, the product SS^T equals the identity plus a term that is annihilated by the projection operators in Eq. 36. Because of this property, the dimensionality of all the filter equations can be reduced using S and S^T without changing the basic formalism. That is, the Kalman filter equations for the unconstrained 6-component state are formally identical to those for the original 7-component state. Only one extra step (Eq. 57) is required at each update to convert the 6-component error state into the full 7-component state that is needed for the next propagation step. The state error covariance is updated and propagated always in its 6×6 reduced form.

IMPLEMENTATION

The spinning spacecraft EKF has been implemented in MATLAB as a subsystem of the Multimission Spin-Axis Stabilized Spacecraft (MSASS) Attitude Ground Support System (AGSS). The MSASS AGSS has been used for spinning spacecraft mission support for many years at the NASA/Goddard Space Flight Center (GSFC). The new EKF subsystem adds an important capability to solve for a time-dependent attitude history and could be used for real-time applications, if needed.

The software is divided into an MSASS driver, an EKF main routine, and subroutines for time-propagation, computation of the sensitivity matrices, and filter update. The driver collects sensor measurement data and presents it to the filter as vector observations (rate and quaternion sensor data are not yet implemented in MSASS but can be generated in a simulator developed specifically to test the filter). If the commanded control torques are available, these should also be passed to the filter either as magnetic moments or directly as magnetic or thruster torques.

After discarding any points flagged as bad, the EKF main routine checks the observation time steps and will interpose extra propagation steps, as needed, to improve the time-integration between sensor observations. The main routine also obtains the spacecraft ephemeris and geomagnetic field at each integration time step in order to compute environmental torques, if this option in the dynamics model is enabled.

The environmental model includes torques due to gravity gradients and due to any residual constant magnetization of the spacecraft (see, e.g., Ref. 6). The gravity gradient torque can be written

$$\mathbf{N}_{GG} = \frac{3\mu}{r^3} \hat{\mathbf{r}} \times (J \hat{\mathbf{r}}), \quad (58)$$

where \mathbf{r} is the spacecraft position vector, r is its magnitude, $\hat{\mathbf{r}}$ is the corresponding unit vector, J is the spacecraft body frame inertia tensor, and μ is the Earth's gravitational constant. The magnetization torque is simply

$$\mathbf{N}_{mag} = 1 \times 10^{-7} (\mathbf{m} \times \mathbf{B}), \quad (59)$$

where torque is in Newton-meters (N-m), \mathbf{m} is any residual spacecraft magnetic moment in Ampere-meter² (A-m²), and \mathbf{B} is the Earth's magnetic induction in milliGauss (mG).

For each observation, the main routine calls the propagation subroutine to integrate the state vector and its covariance to the observation time. This subroutine uses a 4th-order Runge-Kutta time-integration method. Next, the sensor residual and the appropriate sensitivity matrix are computed, and the state and covariance are updated.

The initial state vector and covariance matrix are input to the EKF using familiar attitude and rate variables. The conversion to Markley variables is performed internally. Similarly, the estimated state and covariance are converted to attitude and rate variables before output. The internal use of Markley variables is totally transparent to the User.

Singularity Avoidance

It is clear throughout the development of this filter that the spacecraft angular momentum must be nonzero, but even with this stipulation, there are two other singularities. First, it can be seen from Eq. 11 that the ζ variable is undefined when $\mathbf{L}_B \cdot \mathbf{L}_I = -L^2$. That is, the \mathbf{L}_B and \mathbf{L}_I vectors cannot be 180 deg apart. For example, the angular momentum in the body frame typically is near the Z-axis. If this is so, this singularity precludes any attitude where the spin axis is at the celestial south pole. The second singularity can be seen in Eq. 38, which is needed to define the reduced representation. Problems occur when the inertial frame angular momentum is near $\pm\mathbf{Z}$, that is, near either celestial pole, regardless of where the angular momentum is in the body frame.

It is an important feature of the software that it checks and maintains itself sufficiently far from these singular points of the representation. Whenever the estimated attitude is closer to any singular point than a user-specified tolerance, the software redefines the inertial reference frame. In this modified inertial frame, \mathbf{L}_I is far from the celestial poles and from $-\mathbf{L}_B$. The software transforms all reference vectors along with \mathbf{L}_I . The inertial frame may be modified repeatedly whenever the solution approaches a singular point. Finally, to reconstruct the usual attitude, it is only a matter of bookkeeping to keep track of the times these extra rotations were applied. These transformations are all handled internally and again are totally transparent to the User.

TEST RESULTS

Simulation Parameters

A variety of tests have been performed using simulated data to exercise all the key features of the filter. The simulation is based on parameters from the THEMIS series of spinning spacecraft. For this mission, the simulation epoch is taken to be January 2, 2006 at 00 hours, 40 minutes, and the orbital parameters at epoch are

semi-major axis	= 43052.445 (km)
eccentricity	= 0.777800
inclination	= 0.16580627893946 (rad)
right asc. of asc. node	= 6.28177128263078 (rad)
argument of perigee	= 0.00276973678203 (rad)
mean anomaly	= 6.27689555620237 (rad)

The initial true anomaly is 355.4 deg.

The initial spin axis is directed 10 deg anti-sunward from the south ecliptic pole; the initial attitude quaternion is taken to be

$$q_0 = [-0.74356587177477; \\ 0.60417508447320; \\ 0.19420186426192; \\ 0.21063688554197] . \quad (60)$$

The spin rate is 20 revolutions per minute (rpm) approximately about the Z-axis. Various nutation angle offsets from the body Z-axis have been assumed for the tests. The moment of inertia tensor ($\text{kg}\cdot\text{m}^2$) for a fully deployed configuration for THEMIS (Ref. 7) has been simplified to be axially symmetric,

$$J_{sim} = \begin{bmatrix} 200 & 0 & 0 \\ 0 & 200 & 0 \\ 0 & 0 & 384 \end{bmatrix} . \quad (61)$$

This simplifies numerical tests where the truth model is derived from closed-form analytic solutions to the dynamics equations. Other tests without axial symmetry and with nonzero off-diagonal terms in the inertia tensor have not caused problems.

The sensor complement for THEMIS is a three-axis magnetometer (TAM) running at 8 observations per second (24 per spin period) and a slit Sun sensor that detects a Sun pulse once per spin and the Sun elevation angle from the nominal spin plane. For the EKF, the Sun elevation measurement and known slit azimuth angle are combined into an observed Sun unit vector. Gyros measure rotation rates about the two axes transverse to the spin during some parts of the mission.

Unless otherwise indicated, the sensor noise in both the truth model and for EKF tuning are 0.1 deg for the Sun sensor elevation, 0.0007 sec for the Sun pulse time, and 1 mG per axis for the magnetometer. These are 1σ values. The magnetometer noise covariance is the square of the ratio of this 1 mG error to the magnitude of the ambient geomagnetic field. The field is approximately 90 mG for the shorter tests and ranges from 90 to 10 mG for the longest runs (note that the orbit is quite eccentric). A rate error of 10^{-4} deg/sec^{1/2} is used for both the truth model and the EKF gyro noise R matrix.

The process noise is taken, somewhat arbitrarily, to be the diagonal matrix

$$Q(t) = \text{diag}(10^{-6}, 10^{-6}, 3 \times 10^{-6}, 10^{-7}, 10^{-7}, 3 \times 10^{-7}) , \quad (62)$$

corresponding to an error growth per hour of roughly 3.4 deg transverse to the spin direction, 5 deg around the spin axis, 1.1 deg/sec transverse rate, and 1.9 deg/sec spin rate. Note that this process noise is transformed on input from attitude and rate noise into the reduced Markley variable representation.

Test 1 – Torque-Free Rotation with Nutation

To justify the added complexity, it must be shown that the new filter performs better than a more conventional quaternion-based filter. There are similarities between the new filter and quaternion-based filters (Ref. 5). In particular, the attitude and rate (or gyro rate bias) form a 7-element state vector subject to one constraint condition. In a quaternion-based filter, the constraint is that the quaternion must be normalized. Several of the tests presented here compare results from the new filter and the “unit vector filter” (UVF) (Ref. 8). The UVF has been used for attitude ground support at NASA/GSFC for many three-axis stabilized missions over the past 12 years. For application to spinning spacecraft, the UVF has been modified to estimate the quaternion and rotation rate rather than the gyro biases, to use dynamics propagation rather than gyro propagation, and to include a J -dependent term in the linearized dynamics matrix to be used in Eq. 13:

$$F = \begin{bmatrix} -[\boldsymbol{\omega} \times] & -I \\ \mathbf{0}_{3 \times 3} & J^{-1}([\mathbf{J}\boldsymbol{\omega} \times] - [\boldsymbol{\omega} \times]\mathbf{J}) \end{bmatrix}. \quad (63)$$

The first test scenario is simple torque-free motion with various values for the nutation angle. The filters were given 60 seconds convergence time, and statistics were collected over the next 90 seconds (30 spin periods). Table 1 shows the mean error in the direction of the estimated angular momentum vector and the standard deviation of the error in the rotation phase about the body Z-axis. The new filter is noisier than the UVF in the spin phase estimate. At larger nutation angles, the new filter is slightly better at determining the angular momentum direction (which is operationally the more important statistic for most missions). However, the differences are small and the errors for both filters easily meet the 1 deg mission attitude knowledge requirement expected for THEMIS.

Table 1. Comparison of New Markley Variable Filter and Unit Vector Filter for Torque-Free Nutation.

Nutation Angle (deg)	Mean Error in Ang. Momentum Direction (deg)		Std. Dev. of Error about Body Z-axis (deg)	
	New Filter	UVF	New Filter	UVF
0	0.09	0.09	0.14	0.10
0.5	0.09	0.09	0.15	0.10
1.0	0.09	0.09	0.15	0.10
2.5	0.08	0.09	0.14	0.08
5.0	0.06	0.08	0.15	0.07
7.5	0.07	0.09	0.18	0.07
10.0	0.08	0.10	0.17	0.06

Test 2 – Attitude Reorientation

The new filter behaves very well during large attitude reorientation slews. This test simulates a 90 deg attitude slew over a 230 sec time span. THEMIS is expected to perform large slews such as this during the early part of the mission prior to boom deployment.

The filter followed the changing direction of the angular momentum vector throughout the slew. Figure 1 shows the attitude error relative to the truth model. The error in the estimated direction of the angular momentum, averaged over several runs, is only 0.09 deg during the slew. This is indistinguishable from the errors after slew completion. The errors for these tests using the UVF are 2 times larger, averaging 0.18 deg.

Test 3 – Sensor Misalignments

The TAM on THEMIS will be mounted on a deployable boom. The deployed alignment is expected to be reproducible only to within ± 1 deg. To test how this would affect the attitude, the TAM misalignment was set to +1, +1, and -1 deg on the X-, Y-, and Z-axes. Figure 2 shows a sample of the resulting attitude errors. The mean angular momentum pointing error is only 0.86 deg.

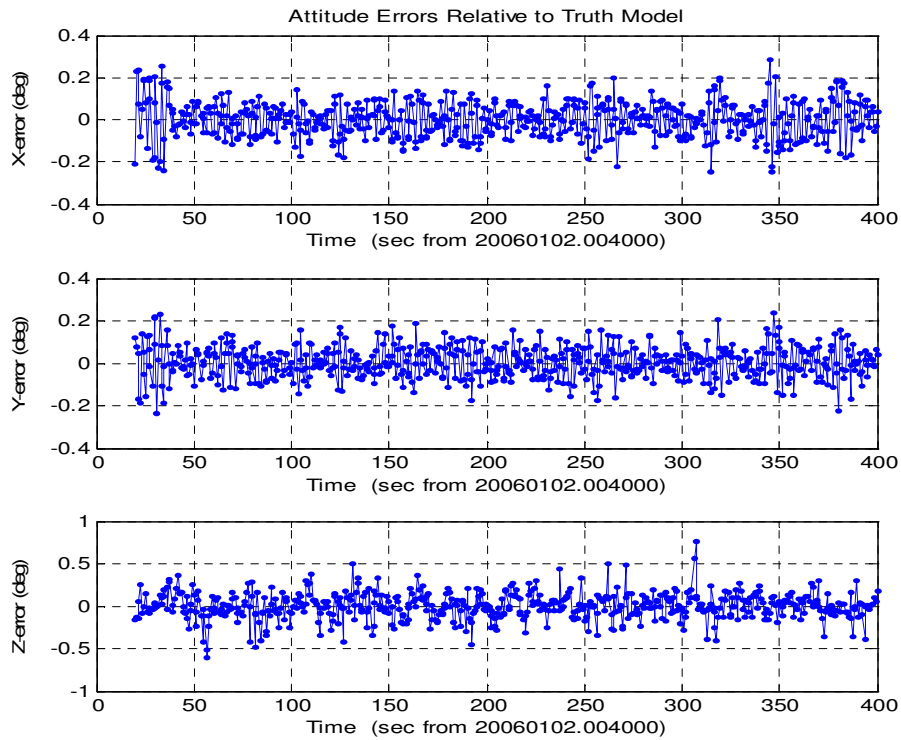


Fig. 1. Attitude errors relative to truth model for a 90 deg slew. The slew ends at 230 seconds. The filter follows the slew with a mean pointing error of only 0.09 deg.

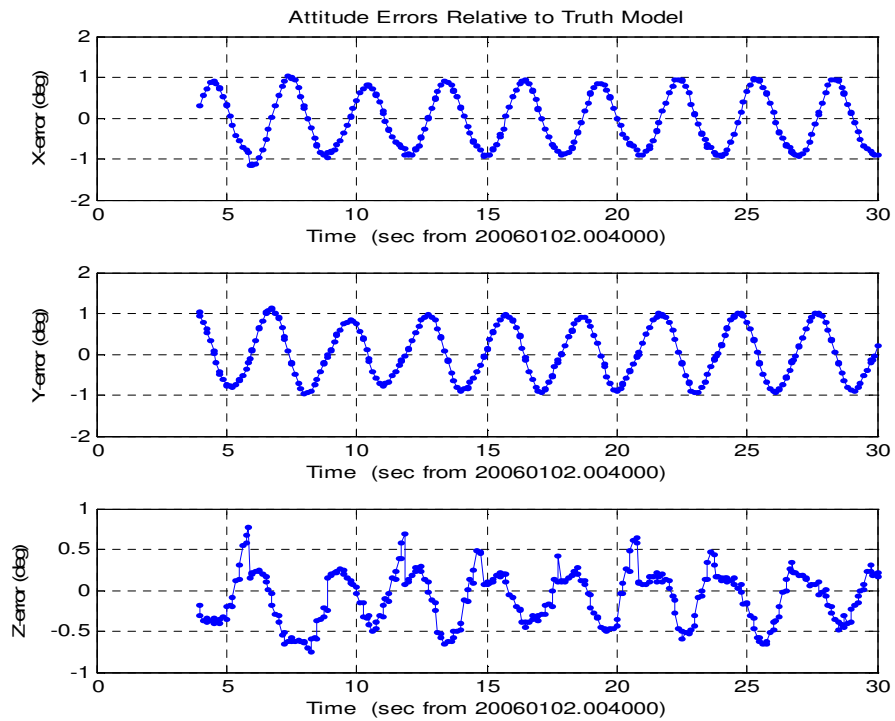


Fig. 2. Attitude errors relative to truth model given a 1 deg misalignment on each TAM axis. The true attitude is modeled by torque-free motion with 5 deg nutation.

When the slit Sun sensor is also shifted by 1 deg in azimuth and 1 deg in elevation, the mean attitude errors are found to range between 0.5 to 1.9 deg, depending on the signs of the misalignment angles. The wide range occurs because the systematic errors from the Sun sensor misalignment can add to or subtract from those of the TAM. The errors with the UVF were similar.

Test 4 – Sensor Complement

This test investigates how performance varies with the data frequency of the TAM and with the availability of the two-axis gyro measurements. The attitude scenario is a 90 deg reorientation as in Test 2.

Table 2 presents test results showing mean angular momentum pointing errors averaged over several runs. The pointing errors are slightly smaller for the new filter, but the difference is barely significant. What is more significant is that the convergence time for the UVF became longer and less predictable as the data frequency decreased. The new filter’s convergence time did not degrade in this way.

The table also shows that using gyro data does not improve the attitude estimation. This may be due to the amount of gyro noise or may indicate filter tuning problems. The gyros do help the filter quickly to converge to the correct rotation rate when initialized with a large rate error (see Test 5).

Perhaps the most interesting result indicated in Table 2 is how well the filter performs even when the TAM data frequency is so low there are fewer than one observation per spin period.

Table 2. Comparison of New Markley Variable Filter and Unit Vector Filter for 90 deg Slew with Various Sensors.

Sensor Complement	Mean Error in Angular Momentum Direction During 90 deg Attitude Reorientation Slew (deg)	
	New Filter	UVF
Sun sensor, 8 Hz TAM, 4 Hz x- and y-axis gyro	0.09	0.18
Sun sensor, 8 Hz TAM, no gyro	0.09	0.10
Sun sensor, 1 Hz TAM, 4 Hz x- and y-axis gyro	0.13	0.20
Sun sensor, 1 Hz TAM, no gyro	0.13	0.16
Sun sensor, 1/3 Hz TAM, 4 Hz x- and y-axis gyro	0.21	0.24
Sun sensor, 1/3 Hz TAM, no gyro	0.17	0.16
Sun sensor, 0.1 Hz TAM, 4 Hz x- and y-axis gyro	0.21	0.28
Sun sensor, 0.1 Hz TAM, no gyro	0.27	0.34

The THEMIS orbit is very eccentric and has a large semimajor axis. The geomagnetic field is relatively weak over most of the orbit and will be useful as an attitude measurement only near perigee. For much of the orbit, the reference field model errors will be too large compared to the field magnitudes for TAM observations to provide attitude information. Two tests were performed to examine the effect of not having input from the TAM. First, a reorientation slew test was performed using only Sun and X,Y-gyro data. The filter was allowed to converge using TAM data, but the TAM was disabled during most of the slew. The new filter again performed better than the UVF. The error in the angular momentum direction after the slew averaged 0.47 deg for the new filter and 0.85 deg for the UVF. In the next test, the filter was allowed to converge using Sun and TAM data for 200 seconds. The motion was torque-free with various nutation angles from zero to 2 deg. Solutions were obtained using only Sun sensor data for the next several thousand seconds. The error growth could easily be kept under a few degrees by choosing the dynamics integration step size. However, it was most surprising that the UVF performed much better for these torque-free Sun-only tests. For a 4000 sec test with 1 deg nutation angle, the UVF showed no error growth compared to Sun and TAM solutions, while the new filter showed linear error growth.

Test 5 – Convergence Tests

The final series of tests examined how reliably the filter converges when initialized far from the true state. Over 50 runs were performed with a wide sampling of large initial attitude errors. In most of these cases, the initial attitude errors were between 90 and 180 deg. Both the new filter and the UVF converged to within 0.3 deg of the true attitude in less than 2 minutes (40 spin periods). Most cases took less than 30 seconds to converge, with only a small number taking the full 2 minutes.

When both the attitude and rate were initialized with large errors, the filters still usually converged quickly. Both filters converged within 2 minutes when the initial rotation rate error was 15 percent on the spin axis and 200 percent on the X- and Y-axes with 90 to 180 deg initial attitude errors.

If gyro data is not included, there are some extreme cases where the new filter did not converge within 4 minutes. In these tests, the initial X- and Y-rate errors were 300 percent of the true rate and the initial attitude error was over 90 deg. With gyro data, even these difficult cases converged quickly.

CONCLUSIONS

The new spinning spacecraft EKF has been shown to perform well under several test scenarios. Its initial convergence is very robust and the overall accuracy is good. However, the filter does not perform significantly better than a more conventional quaternion-based filter such as the UVF. Additional tests and work on the software will look into whether improvements can be made that bring the new filter up to its original expectations. Regardless, this work has succeeded in providing two powerful filters for attitude determination. This adds a significant new capability to the attitude ground support system used for spinning spacecraft missions at the NASA Goddard Space Flight Center.

Ongoing work is investigating how to determine sensor biases, scale factors, misalignments, and time-tag errors, either along with the attitude state or in a parallel utility. Several types of biases are already estimated as part of the current batch-method spinning spacecraft attitude ground support system, where the spin vector is assumed to be constant for the entire batch. However, it may be useful for early mission support to be able to determine the biases before the rotation has fully damped down to simple principal axis spin.

REFERENCES

1. F.L. Markley, "New Dynamic Variables for Rotating Spacecraft," AAS-93-330, *Proceedings of the International Symposium on Spaceflight Dynamics*, NASA/GSFC, Greenbelt, MD, Advances in the Astronautical Sciences, Vol. 84, Univelt, San Diego, 1993
2. J. Sedlak, "Kalman Filter Estimation of Spinning Spacecraft Attitude Using Markley Variables," *Proceedings of the 18th International Symposium on Spaceflight Dynamics*, Munich, Germany, 2004 [however, the current paper gives corrected equations, as noted]
3. M.D. Shuster, "A Survey of Attitude Representations," *Journal of the Astronautical Sciences*, Vol. 41, No. 4, Oct.-Dec. 1993, pp. 439-517
4. A. Gelb, ed., *Applied Optimal Estimation*, MIT Press, Cambridge, MA, 1974
5. E.J. Lefferts, F.L. Markley, and M.D. Shuster, "Kalman Filtering for Spacecraft Attitude Estimation," *J. Guidance, Control, and Dynamics*, Vol. 5, No. 5, Sept.-Oct. 1982, pp. 417-429
6. J.R. Wertz (ed.), *Spacecraft Attitude Determination and Control*, D. Reidel Publishing Company, Dordrecht, The Netherlands, 1978, p. 567
7. R. LeBoeuf, C. Woodruff, and K. London, *THEMIS Mission Critical Design Review Attitude Control System*, Swales Aerospace, WBS Element 00536.2.2.2.1.1, June 16, 2004
8. J. Sedlak and D. Chu, "Kalman Filter Estimation of Attitude and Gyro Bias with the QUEST Observation Model," AAS 93-297, *Proceedings of the AAS/GSFC International Symposium on Space Flight Dynamics*, Greenbelt, MD, 1993